Electronic supplementary information

Adsorption of cesium and strontium on mesoporous silicas

Kento Murota [a] [*], Yoshio Takahashi [b], Takumi Saito [c]

a Regulatory Standard and Research Department, Secretariat of Nuclear Regulation Authority,

1-9-9 Roppongi, Minato-ku, Tokyo 106-8450, Japan

b Department of Earth and Planetary Science, Graduate School of Science, The University of

Tokyo, 7-3-1 Hongo, Bunkyo-ku, Tokyo 113-0033, Japan

c Nuclear Professional School, School of Engineering, The University of Tokyo, 2-22

Shirakata Shirane, Tokai-mura, Naka-gun, Ibaraki 319-1188, Japan

Corresponding Author

* E-mail: murota_kento_zs6@nra.go.jp

Table S1 Textural properties and surface hydroxyl group densities of mesoporous silicas.[1]

| | MCM-41 | | | SBA-15 | | |
	M3.4	M6.8	M12.4	S7.1	S7.9	S8.2
Mesopore diameter (nm)	3.4	6.8	12.4	7.1	7.9	8.2
Specific surface area (m^2/g)	622	628	431	456	481	535
< 2 nm in diameter (m^2/g)	32	414	94	232	246	252
> 2 nm in diameter (m^2/g)	589	214	337	224	236	284
Surface hydroxyl group density (/nm^2)	3.06	3.02	4.81	4.89	3.94	4.16
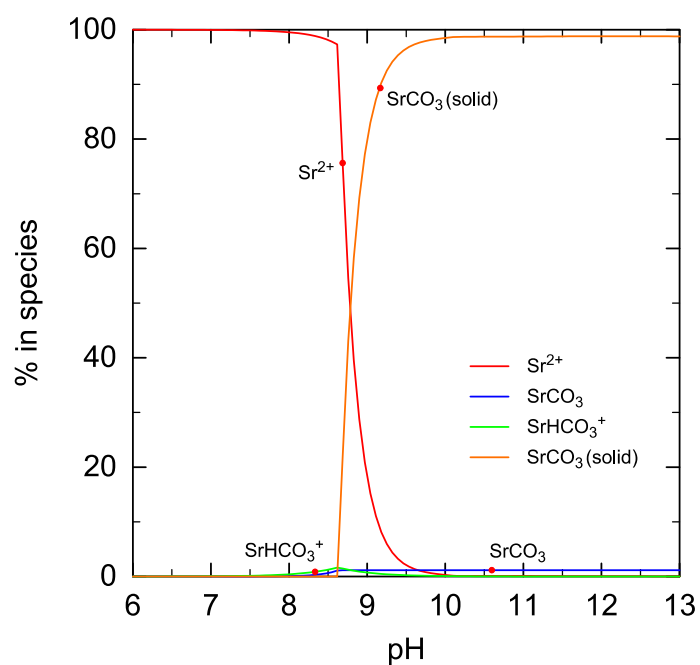
Fig. S1 Speciation of Sr^{2+} in the absence of adsorption on silica surface calculated by PHREEQC.
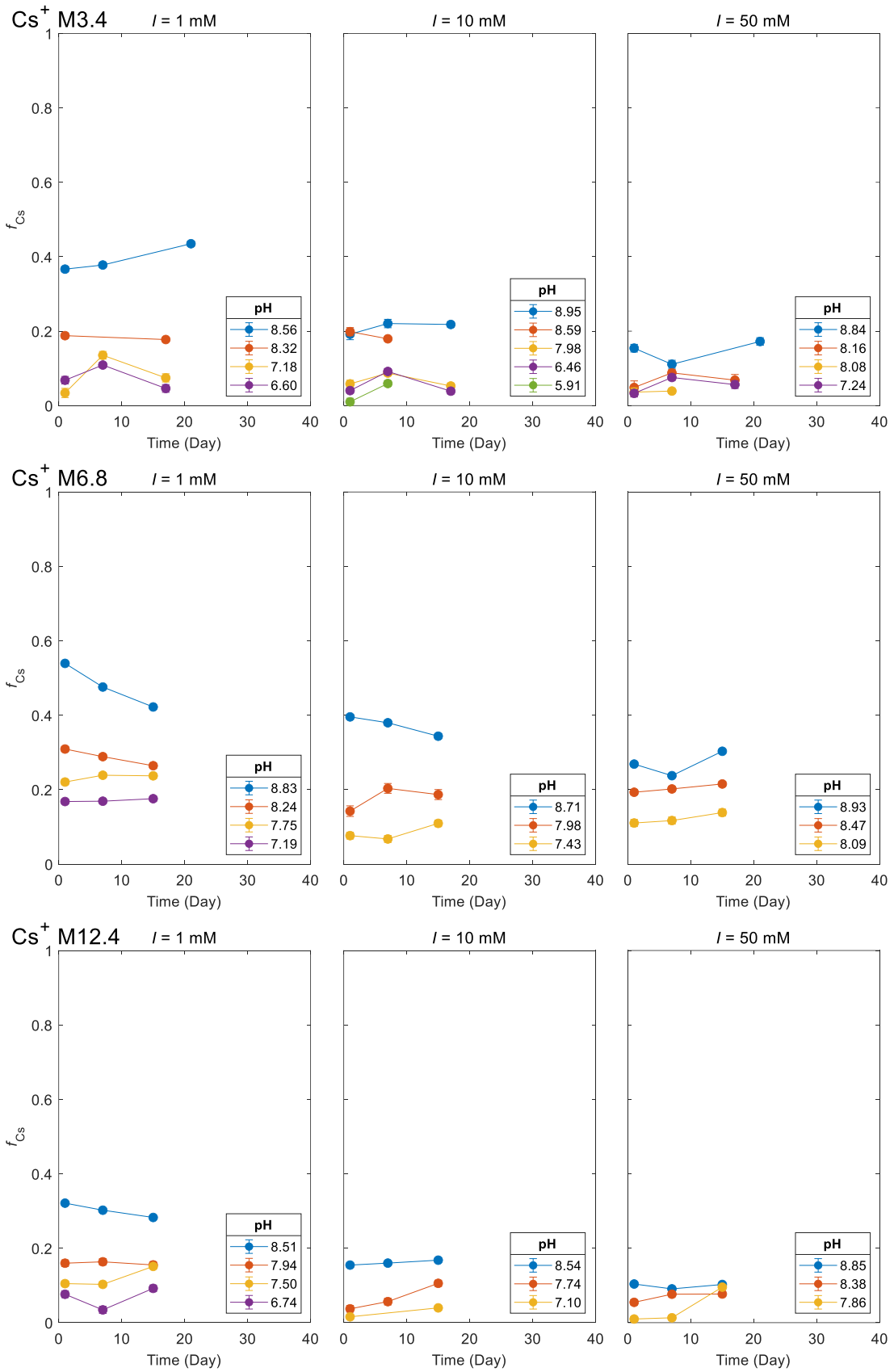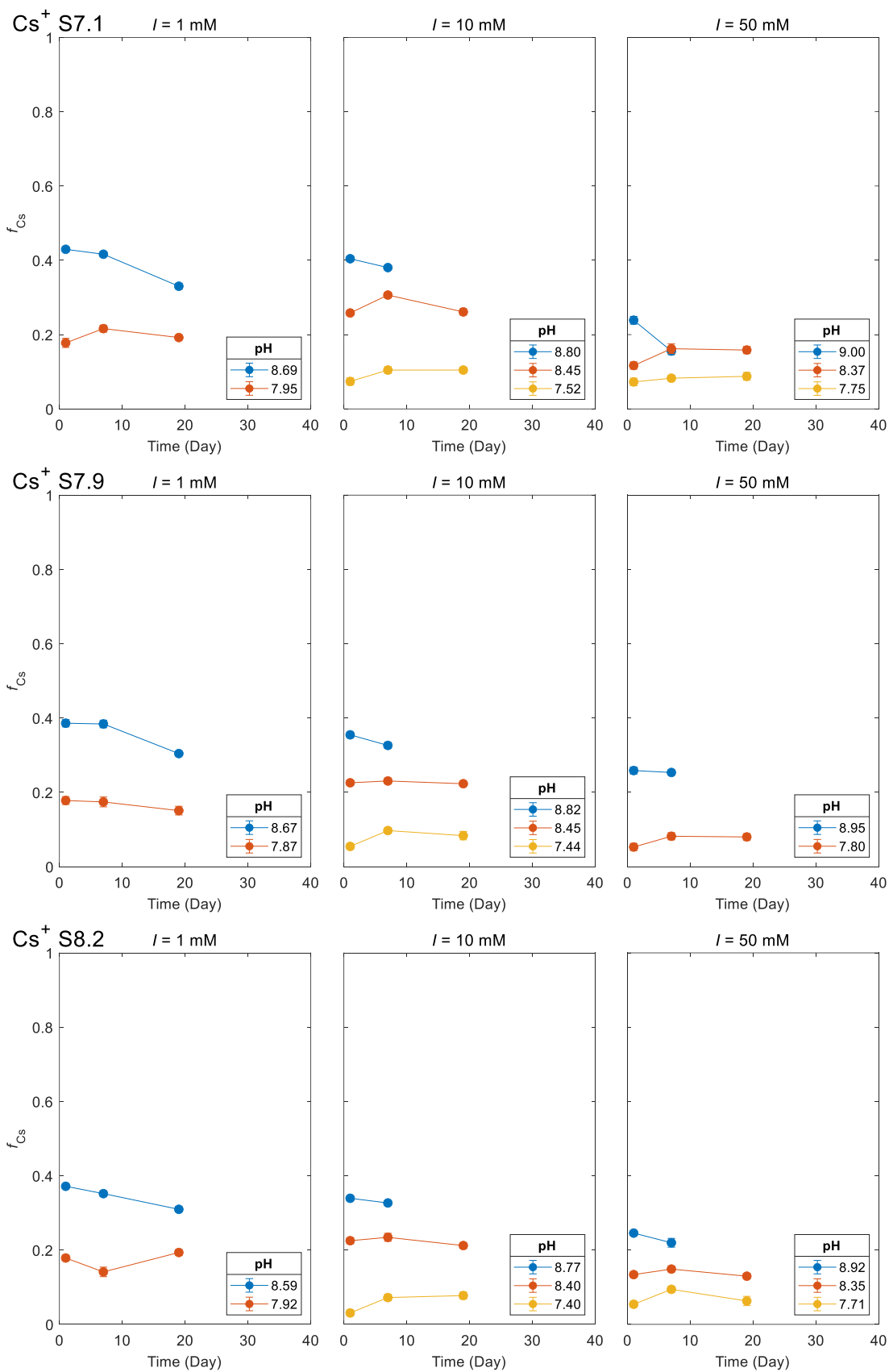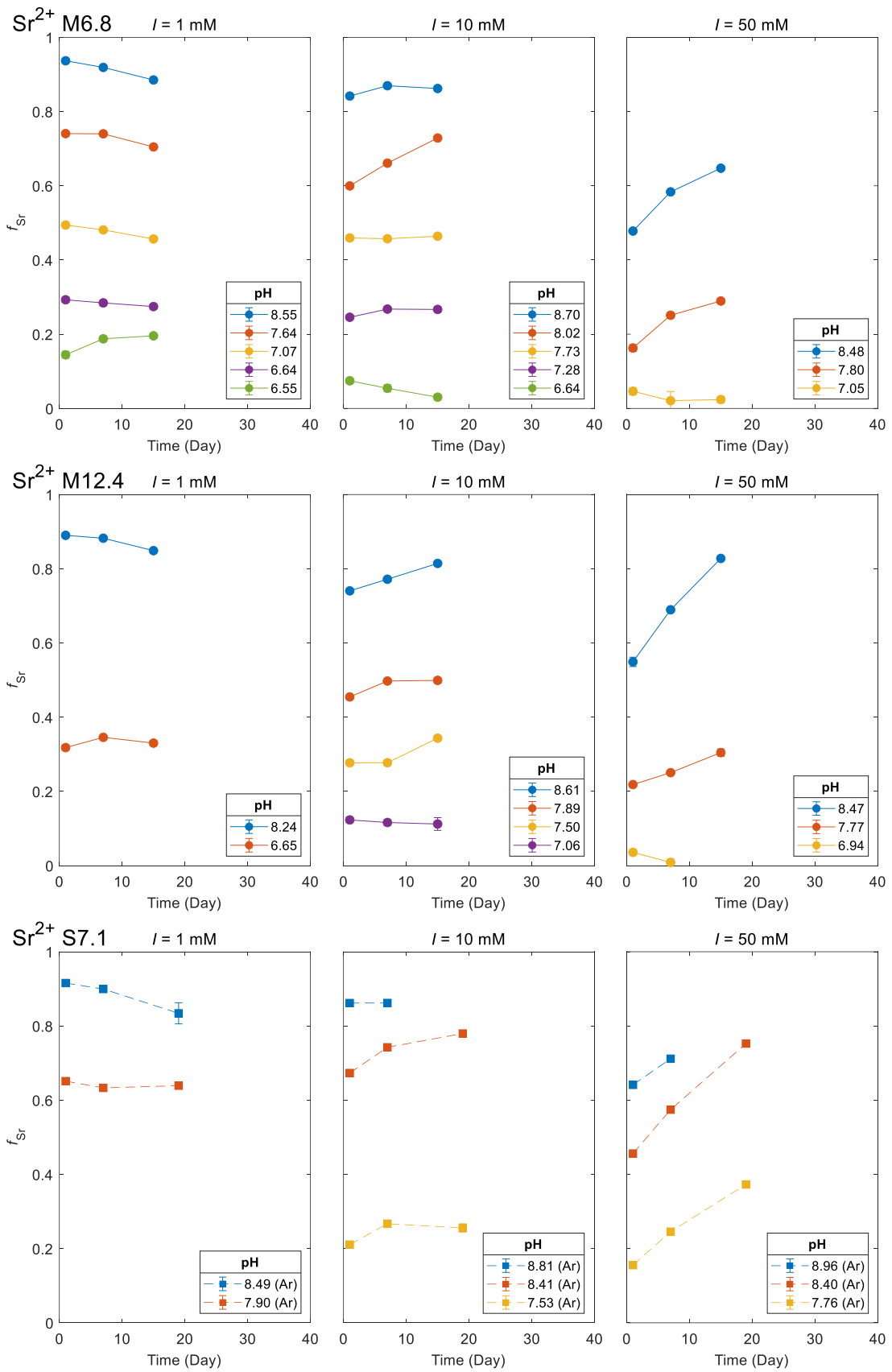
Fig. S2 Time variation of adsorbed fractions of Cs^+ (f_{Cs}) on the six mesoporous silicas at different pH and ionic strengths of 1, 10, and 50 mM.
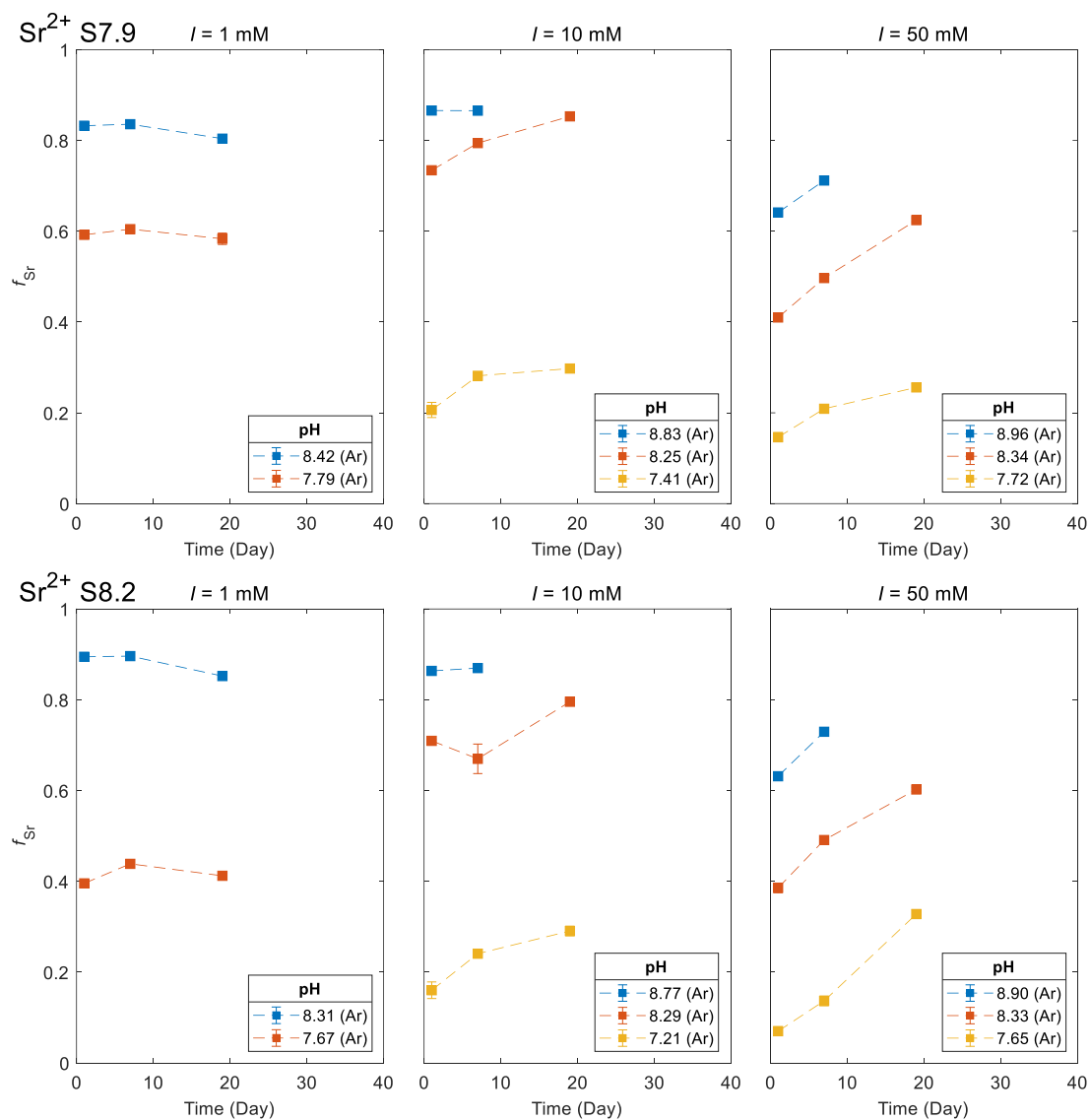
Fig. S3 Time variation of adsorbed fractions of Sr^{2+} (f_{Sr}) on the mesoporous silicas other than M3.4 at different pH and ionic strengths of 1, 10, and 50 mM. The results shown by the dashed line were obtained in an argon atmosphere.
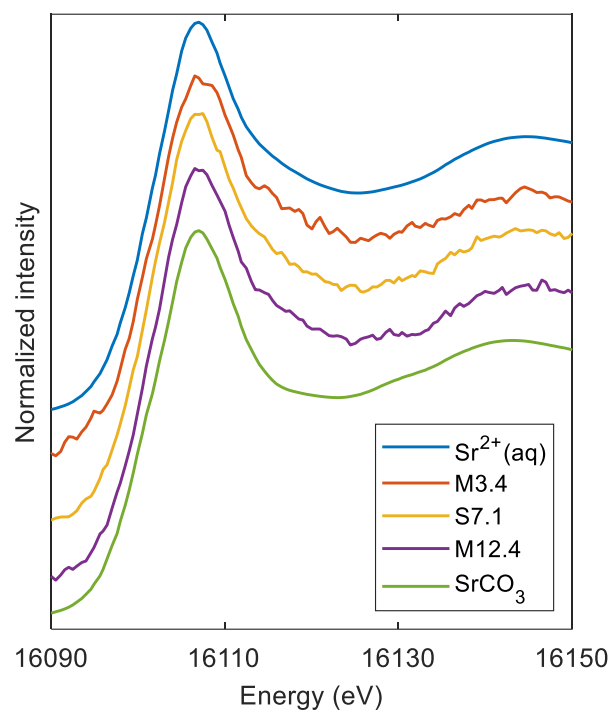
Fig. S4 Sr K-edge XANES spectra of Sr^{2+} adsorbed on three types of mesoporous silicas.
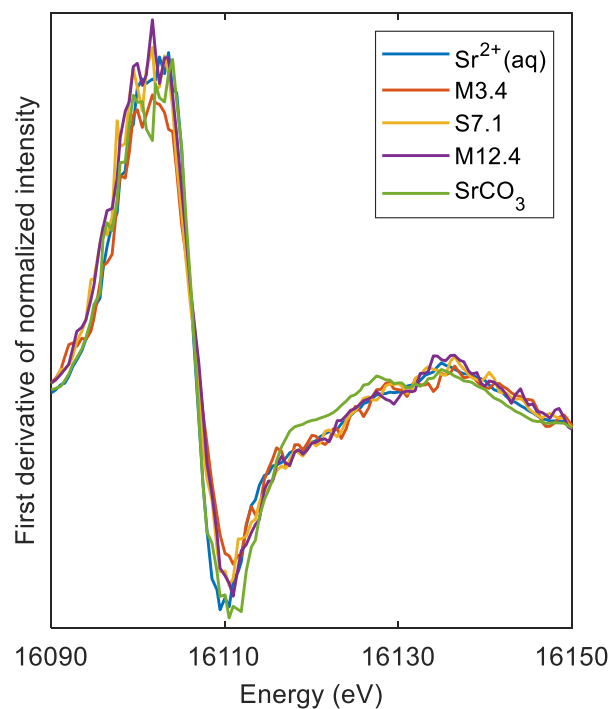

Fig. S5 First derivatives of Sr K-edge XANES spectra of Sr^{2+} adsorbed on three types of mesoporous silicas.
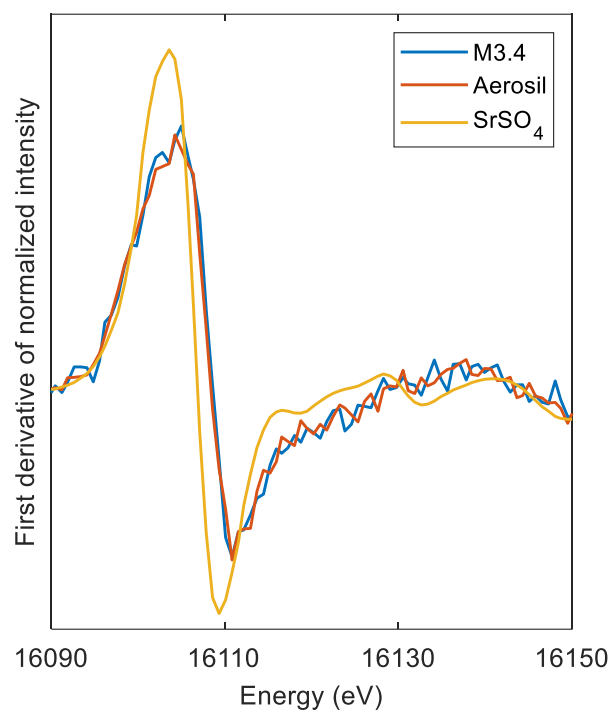
Fig. S6 First derivatives of Sr K-edge XANES spectra of Sr^{2+} adsorbed on M3.4 and Aerosil OX50.
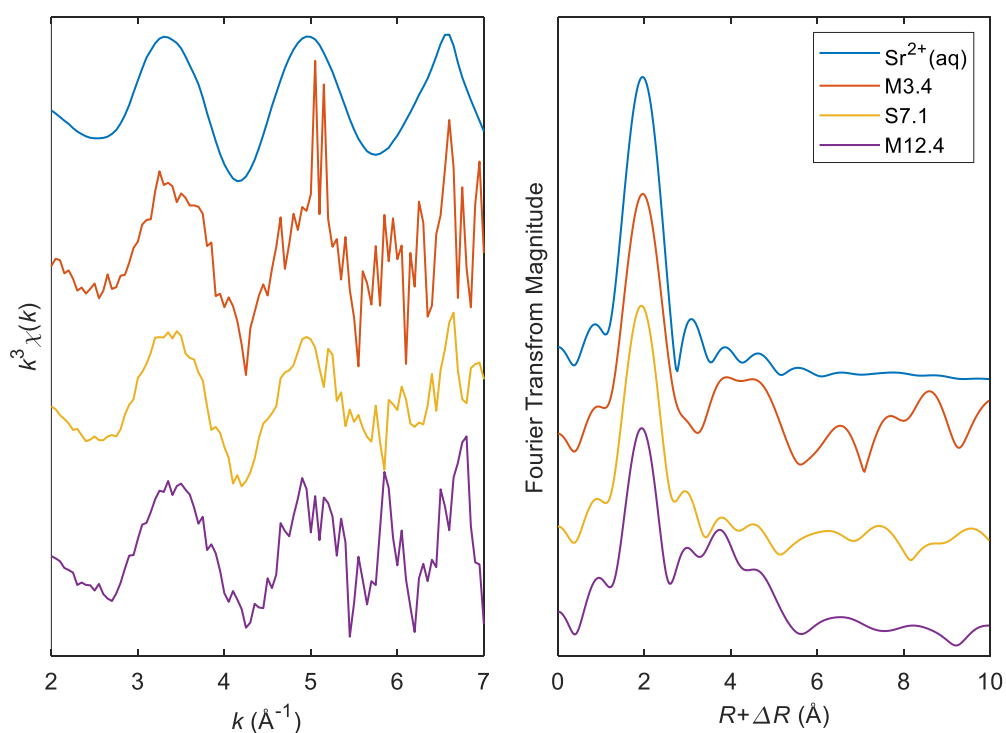

Fig. S7 k^3-weighted Sr K-edge EXAFS spectra ($k^3\chi(k)$) (left) and their Fourier transforms (right) of Sr^{2+} adsorbed on three types of mesoporous silicas.
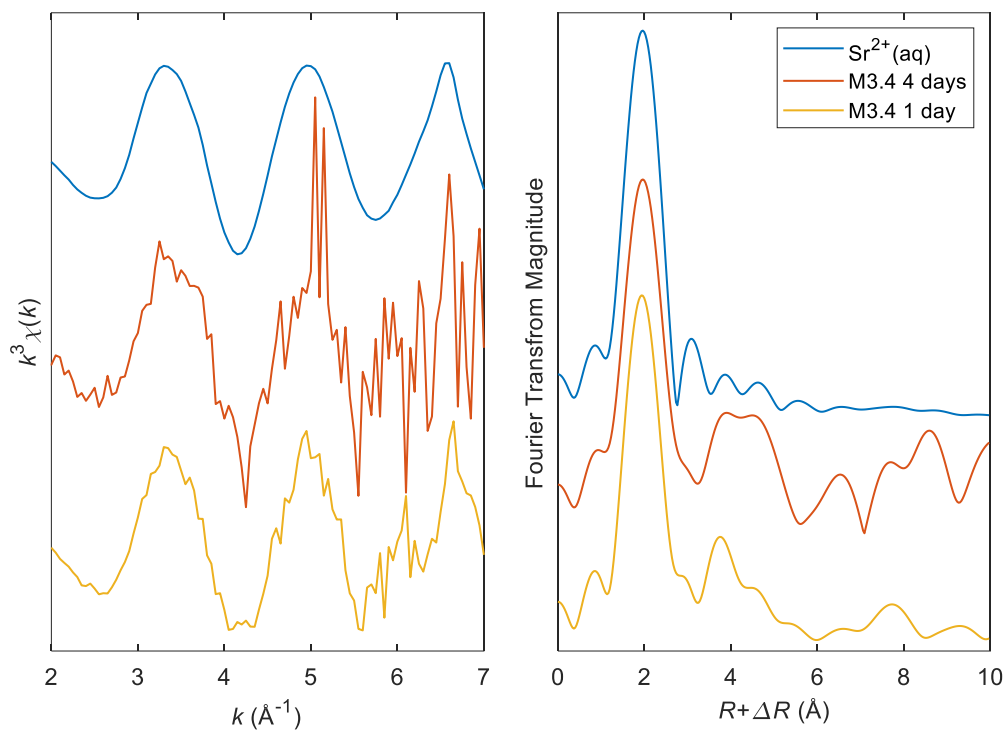
Fig. S8 k^3-weighted Sr K-edge EXAFS spectra ($k^3\chi(k)$) (left) and their Fourier transforms (right) of Sr^{2+} adsorbed on M3.4 for 1 or 4 days.

Table S2 Capacitances of the Stern layer of pores with different diameters optimized by the fitting of the surface complexation model to the surface charge densities.[1]

Pore diameter (nm)	1.36	3.4	6.8	12.4	7.1	7.9	8.2
Capacitance (F/m^2)	0.56	1.05	5.58	3.80	4.53	2.27	4.04
95% confidential interval (F/m^2)	0.36	0.11	9.61	1.84	3.30	1.17	1.15

Charge distribution model

The outer-sphere complexation reactions of Cs^+ (eqn (6) in the main text) assume that the adsorbed Cs^+ resides on the outer Helmholtz plane (OHP). The distance of the OHP from the pore surface (the thickness of the Stern layer) is considered the sum of the thickness of the aligned water molecules in the Stern layer and the radius of the hydrated electrolyte ions adsorbed at the OHP.[2,3] When Cs^+, which has a smaller hydration radius than Na^+, forms outer-sphere complexes with the silica surface, adsorbed Cs^+ is thought to be closer to the pore surface than the OHP, whose position is determined by the hydration radius of Na^+. In this case, it is necessary to calculate the adsorption reaction based on the potential corresponding to the position of adsorbed Cs^+. Furthermore, the potential at the position of adsorbed Cs^+ may change with the pore size because the relative permittivity of water near the pore surface changes with the pore size.[1] Therefore, a model considering the distance of the adsorbed Cs^+ from the pore surface was developed and fitted to the experimental results.

The model distributed the charge of Cs^+ between the pore surface and OHP with a ratio f_{charge} according to the distance of the adsorbed Cs^+ from the surface (**Fig. S6**).[4] In this case, $\log K_{int}$ at each plane was assumed to be the same, but the apparent equilibrium constant (K_{app}) changes as the potential ($\psi_x = \psi_{surface}$ or ψ_{OHP}) changes.

$$K_{app} = K_{int} \exp\left(-\frac{\Delta z F \psi_x}{RT}\right), \tag{S1}$$

where Δz denotes the charge difference generated by adsorption, F represents Faraday's constant, R represents the gas constant, and T represents the temperature.
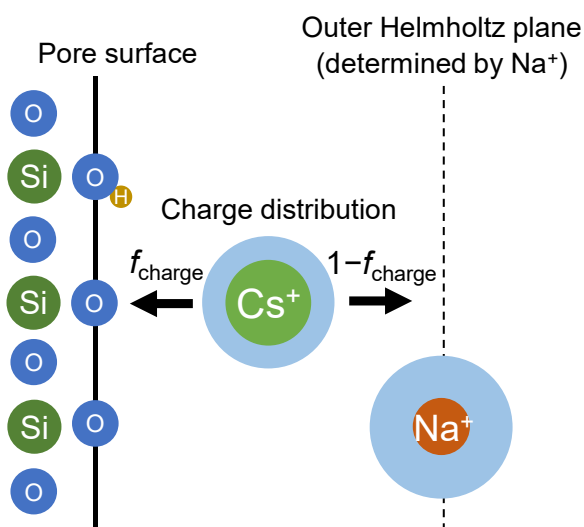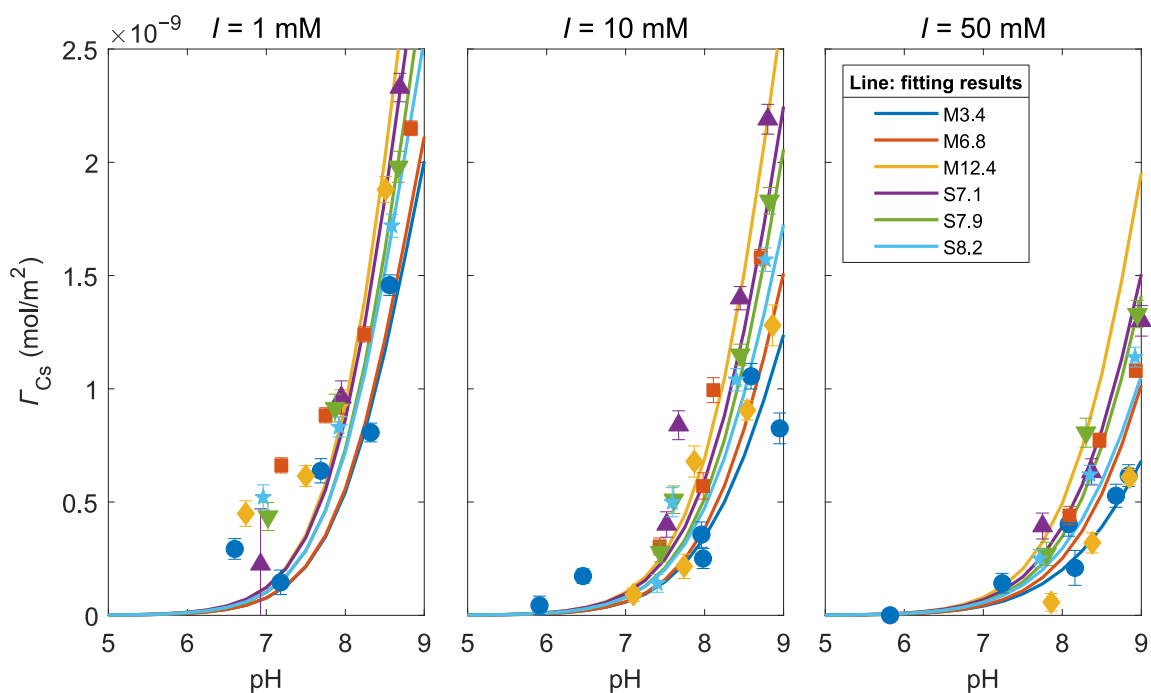

Fig. S9 Conceptual diagram of the charge distribution model.

Fig. S10 Fitting results for adsorbed amount of Cs$^+$ per unit surface area (Γ_{Cs}) obtained from the adsorption experiments, with a common intrinsic equilibrium constant for the different sized pores.
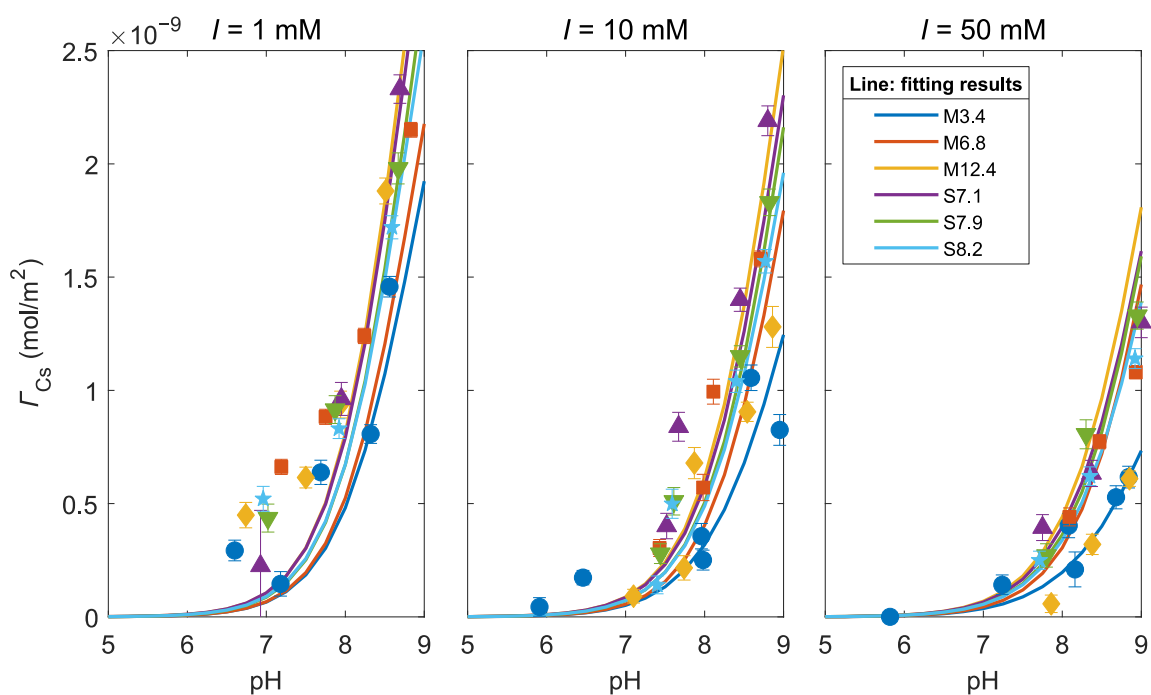

Fig. S11 Fitting results for adsorbed amount of Cs$^+$ per unit surface area (Γ_{Cs}) obtained from the adsorption experiments, with a common intrinsic equilibrium constant and different charge distribution fractions for the different sized pores.

Table S3 Charge distribution fractions f_{charge} for different sized pores optimized by the fitting.

Pore diameter (nm)	f_{charge}
1.36	0.3 ± 1.6
3.4	0.1 ± 0.4
7.1	0.1 ± 1.6
7.9	0.3 ± 1.6
8.2	0.3 ± 1.1
6.8	1.0 ± 2.5
12.4	0.0 ± 0.6

A possible cause of the discrepancy between the experimental and model results

The possible cause of the discrepancy between the experimental and model results is the contribution of Cs^+ or Sr^{2+} not adsorbed on the pore surface but present inside the pore.

The overlap of the electrical double layer in nano-sized pores decreases the electrostatic potential (ψ_{pore}) inside the pore.[1] Therefore, the Cs^+ or Sr^{2+} concentration inside the pore (C_{pore}) would be larger than that in the bulk solution (C_{balk}). When the solution inside the pore and bulk solution are in chemical equilibrium (Gibbs free energies of the two are equal), it is called Donnan equilibrium, and the following equation holds.[5]

$$RT \ln\left(\frac{C_{balk}}{C_0}\right) = RT \ln\left(\frac{C_{pore}}{C_0}\right) + zF\psi_{pore}, \tag{S2}$$

where C_0 denotes the concentration in the standard state (1 M). The potential at the center of the pore with a diameter of 10 nm is calculated to be approximately -0.1 V At an ionic strength of 1 mM by the cylindrical one-dimensional Poisson–Boltzmann equation.[1] Assuming that the whole pore has this potential, the ratio C_{pore}/C_{balk} is approximately 49 for Cs^+, confirming that a concentration difference occurs between the inside and outside of the pore. The calculated Γ from the results of adsorption experiments based on eqn (1) in the main text includes the difference in the concentration of Cs^+ or Sr^{2+} between the inside and outside of the pore. This explanation is supported by the fact that the discrepancy between the experimental and model results was significant at low ionic strengths when the potential inside the pores decreases significantly because of the overlap of the electrical double layer. In addition, it is reasonable that the discrepancy between the experimental and calculated results was greater for Sr^{2+} (**Fig. 2**) than for Cs^+ (**Fig. 1**) because C_{pore}/C_{balk} increases to the square as the valence increases from one to two.
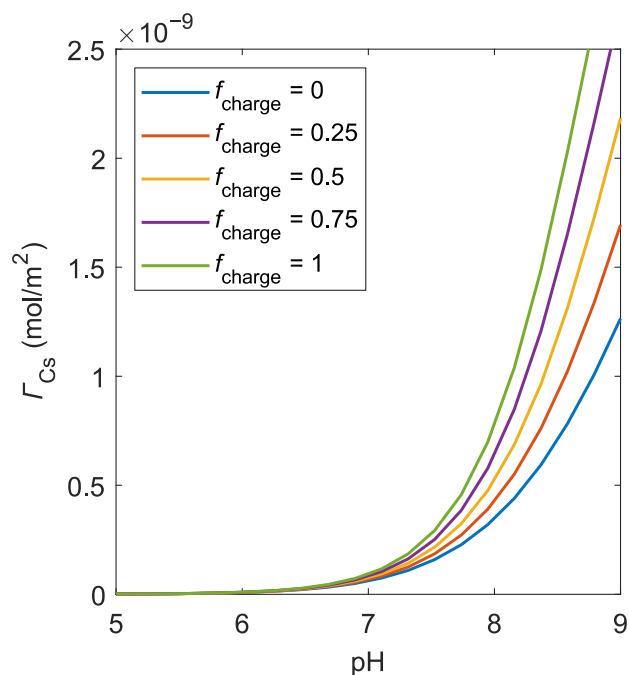
Fig. S12 Calculated adsorbed amount of Cs$^+$ per unit surface area (Γ_{Cs}) for different charge distribution fractions f_{charge}. Pore diameter, ionic strength, capacitance of Stern layer, surface hydroxyl density, and $\log K_{int}$ were set to 5 nm, 10 mM, 1 C/m^2, 4 /nm^2, and 0.7, respectively.
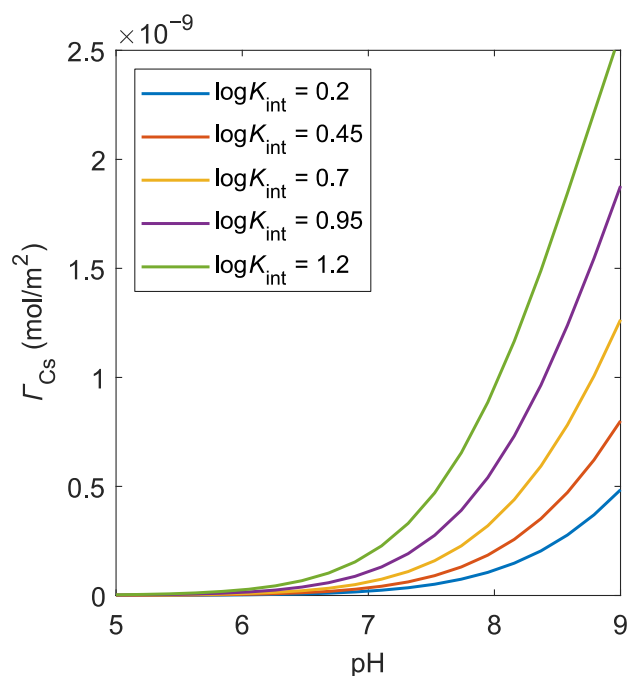

Fig. S13 Calculated adsorbed amount of Cs$^+$ per unit surface area (Γ_{Cs}) for different $\log K_{int}$. Pore diameter, ionic strength, capacitance of Stern layer, and surface hydroxyl density were set to 5 nm, 10 mM, 1 C/m^2, and 4 /nm^2, respectively.

References in the Supplementary material

1   K. Murota and T. Saito, Pore size effects on surface charges and interfacial electrostatics of mesoporous silicas, *Phys. Chem. Chem. Phys.*, 2022, **24**, 18073–18082.

2   D. A. Sverjensky, Interpretation and prediction of triple-layer model capacitances and the structure of the oxide-electrolyte-water interface, *Geochim. Cosmochim. Acta*, 2001, **65**, 3643–3655.

3   M. A. Brown, Z. Abbas, A. Kleibert, R. G. Green, A. Goel, S. May and T. M. Squires, Determination of surface potential and electrical double-layer structure at the aqueous electrolyte-nanoparticle interface, *Phys. Rev. X*, 2016, **6**, 1–12.

4   R. Rahnemaie, T. Hiemstra and W. H. Van Riemsdijk, A new surface structural approach to ion adsorption: Tracing the location of electrolyte ions, *J. Colloid Interface Sci.*, 2006, **293**, 312–321.

5   R. B. Schoch, J. Han and P. Renaud, Transport phenomena in nanofluidics, *Rev. Mod. Phys.*, 2008, **80**, 839–883.